Do all ceramic and composite CAD-CAM materials exhibit equal bonding properties to implant Ti-base materials?

An Interfacial Fracture Toughness study

Abstract

Objectives

To compare the interfacial fracture toughness (IFT) with or without aging, of four different classes of CAD-CAM ceramic and composite materials bonded with self-adhesive resin cement to titanium alloy characteristic of implant abutments.

Methods

High translucent zirconia (Katana; KAT), lithium disilicate-based glass-ceramic (IPS. emax.CAD; EMX), polymer-infiltrated ceramic network material (PICN) (Vita Enamic; ENA), and dispersed filler composite (Cerasmart 270; CER) were cut into equilateral triangular prisms and bonded to titanium prisms with identical dimensions using Panavia SA cement. The surfaces were pretreated following the manufacturers' recommendations and developed interfacial area ratio (Sdr) of the pretreated surfaces was measured. IFT was determined using the Notchless Triangular Prism test in a water bath at 36°C before and after thermocycling (10,000 cycles) (n=40 samples/material).

Results

IFT of the materials ranged from 0.80 ± 0.25 to 1.10 ± 0.21 MPa.m$^{1/2}$ before thermocycling and from 0.71 ± 0.24 to 1.02 ± 0.25 MPa.m$^{1/2}$ after thermocycling. There was a statistical difference between IFT of CER and the two top performers in each scenario: KAT and EMX before aging, and KAT and ENA after aging. Thermocycling significantly decreased IFT of EMX. The Weibull modulus of IFT was similar for all materials and remained so after thermocycling. Sdr measurements revealed that ENA (7.60)>Ti (4.97)>CER (2.85)>KAT (1.09)=EMX (0.96).

Significance

Dispersed filler CAD-CAM composite showed lower performance than the other materials. Aging only affected IFT of Li-Si glass-ceramic, whereas zirconia and PICN performed equally well, probably due to their chemical bonding potential and surface roughness respectively.

Keywords: dental materials, prosthetic dentistry, fracture mechanics, hybrid ceramics, adhesion, cementation, implant prostheses.

Introduction

The manufacture of implant-supported dental prostheses has evolved towards a fully digital workflow using CAD-CAM technology, and a wide range of ceramic and composite materials developed to produce monolithic restorations, which are fabricated at the dental lab or chairside [1–4].

Among ceramics, glass-ceramics, such as lithium disilicates (LiSi), provide excellent esthetics and have shown high strength values and life expectancies [5,6]. Likewise, the market for zirconia is growing exponentially, especially with the evolution of monolithic high-translucent zirconia, which has made it possible to restore anterior teeth [7,8]. Yet, the newest member in the CAD-CAM family includes composites. Despite their lower mechanical properties compared to zirconia and LiSi, CAD-CAM composites possess other advantages, such as better machinability, faster milling rate, longer bur lifetime, and the absence of an additional firing process [9–11]. Moreover, it is possible to mill them to extremely low thickness, and if needed, they can be easily repaired by adding direct composite [12,13].

CAD-CAM composites can be further subdivided according to microstructure into dispersed fillers (DF) composites and polymer-infiltrated ceramic network materials (PICN or "hybrid ceramics") [14]. The former is composed of randomly dispersed fillers in an organic matrix polymerized at high temperature (>100°C), while the latter consists of a pre-sintered ceramic scaffold infiltrated with monomers and polymerized at high temperature and pressure (180°C–300 MPa) [15]. Since the process is patented, the only PICN on the market is Vita Enamic (ENA) (Vita Zahnfabrik, Bad Säckingen, Germany).

For implant-supported prostheses, a titanium abutment (Ti-base) is used to connect the ceramic or composite CAD-CAM material to the implant, in which the restoration is either bonded, screwed or friction-fixed. Recommended bonding systems include self-adhesive resin cements,

that provide ease of use since surface pretreatment procedures are limited. However, a commonly reported problem is debonding of the restoration from the Ti-base, which is found to be one of the most common complications for monolithic ceramic implant-borne single crowns and fixed partial dentures [16–18]. This problem has been reported in different clinical studies with various types of crowns and titanium abutment materials; in many of those studies, the debonding would arise as early as during the initial 1-2 years of clinical aging [19–21]. In some cases, the bonding procedure can be repeated, in some others the restoration moved on the Ti-base but could not be removed from it without being damaged and, indeed, replacement constitutes a major failure and an economical issue for the practitioner and the patient. Oftentimes, patients do not feel the occurrence of a debonding, and the prolonged presence of micromovements and microleakage can be detrimental for the implant and the surrounding tissues stability [22]. Different hypotheses have been formulated to explain observed debonding failures, such as the elastic modulus mismatch between the crown and the abutment material, which particularly occurs with CAD-CAM composites that exhibit a low modulus as compared to titanium [23].

Conventionally, primers are applied to improve bonding of resin cements to CAD/CAM materials. Primers increase surface wettability and chemical bonding, resulting in a stronger bond [24]. Silane is particularly effective for glass phase materials [25], while MDP is suitable for zirconia and metals such as titanium that form an oxide film on their surface [26]. However, the trend in clinical practice is to simplify bonding procedures by using self-adhesive resin cements that are claimed to bond effectively to all materials, including metals, glass-ceramics, composites and zirconia, without the need for a primer [27]. In fact, newer self-adhesive resin cements contain both silane and MDP. However, as MDP is acidic, it accelerates the hydrolysis and self-condensation of silane during storage. This makes the combination of silane and MDP in one bottle less effective [28,29]. In newer products, these components are stored separately

and then mixed in a self-mixing syringe prior to bonding. Many recent self-adhesive cements are also called "universal", meaning that they can be used in both self-adhesive and etch-and-rinse modes [27]. Self-adhesive resin cements are easy for the dental technician to use when bonding a CAD-CAM material to a Ti-base. However, clinical evidence about recent universal products is limited [27]. Furthermore, the available *in vitro* studies do not provide conclusive interpretations. For example, the study by Yoshihara et al [30] shows that Panavia Self Adhesive Cement Universal (PSU) (Kuraray Noritake, Tokyo, Japan) performs comparably to the standard approach (application of a silane primer) with leucite-reinforced glass-ceramic. However, when bonding lithium disilicate glass-ceramics, the use of a silane primer appears to give significantly better results than when used alone [31]. For zirconia, a previous study showed that the use of a self-adhesive resin cement containing MDP (Panavia SA Cement Plus, Kuraray Noritake) with translucent zirconia (Katana Zirconia, Kuraray Noritake) gave better results than the use of a resin cement without MDP but with a separate MDP primer (Panavia V5, Kuraray Noritake) [32].

Various *in vitro* studies have been performed on the bonding properties to Ti-base with zirconia restorations [33–39]. To a lesser extent, other materials such as lithium disilicate glass-ceramic and PICN have been investigated [22,40–42]. Several *in vitro* studies on bonding to Ti-base adopt a crown-abutment configuration with a pull-out technique. However, this configuration does not allow for the evaluation of the bonding interface alone, since results are influenced by the crown-abutment design [43–45]. Some other studies evaluated the shear bond strength of titanium with zirconia or lithium-based glass-ceramic in function of pretreatment [46–48]. However, the shear test approach has been questioned in the literature [49,50]. On the other hand, fracture mechanics is reputed as one of the most reliable methods to evaluate adhesive interfaces [49–54]. The goal is to stably initiate and propagate a crack through the bonded interface and to measure the resistance to crack-propagation or peeling from the substrate [49].

IFT is advantageous because it evaluates the interface properties rather than the mechanical strength of the entire assembly [54]. The Chevron Notch (CN) method is widely recognized as one of the most widely used techniques for determining the fracture toughness of materials and interfaces. In the CN test, a V-shaped cross section is formed by the intersection of two notches. This design concentrates stress at the apex of the V, where a natural crack initiates and grows stably. One of the key advantages of CN is that it allows the K_{IC} to be determined without the need to accurately measure a pre-crack. However, dental researchers often struggle with the use of the CN configuration because it is not possible to create a chevron notch with diamond disks [55]. Ruse et al. [56] suggest the use of a notchless triangular prism (NTP) specimen as a simplified derivative of CN. Indeed, when a triangular prism is placed in the designed holder, it replicates the setup of the standard test. The fracture toughness measured using this approach is also highly consistent with that obtained using CN [56]. The simple sample preparation procedure of NTP may help to reduce the risk of material failure during sample preparation. The NTP method has also been used previously to evaluate IFT [32,52,57,58].

To the best of the authors' knowledge, IFT of CAD-CAM materials with titanium alloy remains unexplored. Additionally, because the clinical failure of resin cement in clinics takes significantly longer time than a quasi-static test, it is useful to age the interface prior to IFT testing. Degradation can be conducted in a variety of ways, such as extended exposure to water, thermocycling, or a combination of these methods. Thermal cycling accelerates the aging of dental materials by increasing interface hydrolysis (in warm bath, which is typically 55^{o}C). It also promotes crack propagation due to stress generated from different levels of contraction and expansion during temperature changes, caused by differences in thermal expansion between materials [59].

Therefore, the objective of this study is to evaluate IFT, at mouth temperature, of Ti-base material bonded to four different classes of ceramic and composite CAD-CAM materials. The null hypothesis is that there is no difference in IFT of the different classes bonded to Ti-base. The second hypothesis is that thermocycling does not influence IFT of each tested material.

Materials and methods

2.1. Preparation of samples and study design

All the materials used in this study and their compositions are listed in Table 1 and the study design in Figure 1.

2.1.1. Prism manufacturing

Titanium alloy characteristic of implant Ti-base was supplied as a disk (Scheftner Dental Alloys, Mainz, Germany), which was cut into prisms with a high-speed saw (Isomet; Buehler, Lake Bluff, IL, USA) under continuous water irrigation to produce the prism-shaped samples. Samples were wet-ground into the desired 6.0±0.1 mm long triangular prisms, 6.3±0.2 mm on a side with 220 grit silicon carbide (SiC) paper, at 300 rpm (Struers, Ballerup, Denmark) using a custom-built specimen holder to manufacture titanium prisms. A schematic representation of the prism preparation is provided in Figure 1.

CAD-CAM composite and ceramic blocks were cut using a low-speed saw (Isomet; Buehler, Lake Bluff, IL, USA) under continuous water irrigation at an angle of 60° to produce 4 samples per block. The samples were then ground into the prism-shaped samples with the same dimensions following the same procedure described before. All prisms of the restorative CAD-CAM materials were prepared to fit with ±0.1 mm precision to their titanium counterparts. EMX prisms were prepared in the crystalline intermediary stage and then fired in a dedicated furnace (Programat, Ivoclar Vivadent, Schaan, Liechtenstein) at 820 °C for 10 s (90 °C/min),

followed by 840 °C for 7 min (30 °C/min), according to manufacturer's recommendations. Sintering of KAT was done by heating at a rate of 10°C/min to 1550°C, then holding the temperature for 2 h, and cooling down to room temperature at the same rate (Zyrcomat furnace, Vita Zahnfabrik, BadSäckingen, Germany), according to manufacturer's recommendations.

2.1.2. Surface pretreatment

All bonding surfaces were polished with 1000-grit SiC paper under water cooling using a custom-made metallic device to provide parallelism for the opposing bonded surfaces. Samples were cleaned before surface pretreatments in ethanol (90%) for 3 min in an ultrasonic bath (Vita Sonic II; Vita Zahnfabrik, Bad Säckingen, Germany), followed by drying with oil-free air for 10 s. The surface pretreatments were then performed according to the manufacturer's recommendations for each material. For Ti-base and KAT, sandblasting was applied with 50 μm Al_2O_3 particles (Danville, Zürich, Switzerland) at 2.5 bar for 5 s in a perpendicular direction at 1 cm from the sample (Basic Professional 2942; Renfert, Hilzingen, Germany). CER was sandblasted at 2 bar following the same procedure. ENA was pretreated with 5% hydrofluoric acid (Vita ceramics etch, Vita Zahnfabrik, Bad Säckingen, Germany) for 60 s, while EMX was pretreated for 20 s with 5% hydrofluoric acid (IPS Ceramic, Ivoclar Vivadent, Schaan, Liechtenstein), then washed under running water for another 60 s and air dried. Following the procedures of etching and sandblasting, all the prisms were additionally cleaned ultrasonically in ethanol for 3 min and air dried for 10 s. As recommended by the manufacturer, no silane or ceramic primer was applied since it is integrated in the composition of the self-adhesive resin cement used in this study.

2.1.3. Bonding procedure

Half-prisms of Ti-base were fixed with a custom-made alignment apparatus and the other respective half-prism of the restorative CAD-CAM material was fixed on the opposite side of the alignment apparatus. The metallic fixation system for bonding is supported on a computer-

controlled (SMC 100, Newport Corporation, California, USA) motorized alignment system (Newport Motion Controller), which controls the space between samples during bonding, therefore controlling the cement thickness at a precision of 0.1 μm. The composite cement, Panavia Self Adhesive Cement Universal (PSU) (Kuraray Noritake, Tokyo, Japan**)** was applied to the pretreated surfaces using a plastic spatula, and the prisms were placed in contact with each other, at 50 μm thickness. The cement was then light-cured at high-power (1200 mW/cm2) on the three sides of the prisms in close proximity for 20 s (Bluephase 20i; Ivoclar Vivadent, Schaan, Liechtenstein). An additional 40 s of curing at a distance of 2 mm for each side was performed after removal from the alignment apparatus to ensure optimal curing.

2.1.4. Aging

After bonding, samples (n = 40 per material) were left in water for 24 h at 36°C. The excess cement was removed after 24 h using 1000-grit SiC. These 24-hour-stored samples were divided into two groups. The first group did not receive any further action; the second group was thermocycled at 5-55°C for 10,000 cycles, with a dwelling time of 30 seconds in each temperature stage [60].

2.2. Interfacial fracture toughness testing

IFT testing was performed using NTP test, following the procedure described by Ruse et al. [56]. NTP configuration is shown schematically in Figure 2. Prisms were fixed into one half of a specimen holder, then, using a sharp scalpel, a crack initiation point (~0.1 mm) was made at the bonded interface under a binocular microscope (Light Highlight 3001, Olympus, Tokyo, Japan) at a magnification of ×20. Testing was performed at a cross-head speed of 0.05 mm/min after mounting the samples on a computer-controlled (Bluehill, Instron Canada, Burlington, ON) universal testing machine (Instron model 5565) in a 36°C water bath. The load values at failure were recorded, and IFT was calculated by the formula $K_{IC} = Y^*_{min} P_{max}/DW^{1/2}$, where P_{max} is the maximum load at failure, D is the NTP specimen diameter (12.0 mm), W is the NTP

specimen length (10.8 mm) and Y^*_{min} is the dimensionless stress intensity factor coefficient minimum (28). Broadly, the geometrical function (Y^*_{min}) in the CN method is influenced by the notch parameters (e.g., a_0-to-a_1 ratio), and the specimen geometry (e.g., width-to-diameter ratios) [61]. a_0 represents the distance from the load application line to the chevron tip, while a_1 denotes the distance from the load application line to the bottom of the notch. Ruse et al. [56] calculated that in the NTP configuration, with an a_0-to-a_1 ratio of 0.5 and a width-to-diameter ratio of 0.88, Y^*_{min} corresponds to a value of 28. He validated this calculation by comparing the measured K_{IC} of a referenced material under these conditions with standard CN configurations.

All samples were examined immediately after testing under a digital microscope (VHX-7000, Keyence, Chicago, IL, USA) to identify the failure mode as adhesive, mixed, or cohesive, as described by Scherrer et al. (see Figure 3, modified from ref. [62]). Indeed, cohesive failures in the CAD-CAM material or Ti must be excluded from the data analysis.

2.3. Developed Interfacial Area Ratio (Sdr)

A prism of each of the CAD-CAM restorative materials, as well as the Ti-base, was prepared by cutting and then polishing with 1000-grit SiC paper. The samples were cleaned ultrasonically in ethanol for 3 min, air-dried then each sample was pre-treated with etching or sandblasting replicating the same procedure for bonding. Laser confocal microscopy (VK-X3050 series, Keyence) was used to determine the developed interfacial area ratio (Sdr), which is expressed as the percentage of additional surface area contributed by the texture compared to an ideal plane the size of the measurement region. The Sdr is obtained by calculating the topographical area with respect to this ideal plane and gives the surface enlargement induced by the different pretreatments in order to promote the micromechanical bond. Measurements were conducted using a ×50 objective lens, with only tilt correction applied during data processing. The achieved resolution was 5 nm in the Z direction, with a pitch size of 0.13 µm

in the X-Y direction; the scanning area dimensions for each measurement were 277 µm × 208 µm. Sdr values were determined by averaging five measurements for each sample.

2.4. Statistical analysis

Power size analysis was calculated at 80% power and a significance level of 0.05, and the total number of samples per group was found to be 13 samples; therefore, the number of samples for each group was decided to be 20 samples (n=20/group).

After assumption checks for distribution normality and homogeneity of variances, statistical differences between IFT were analyzed using 1-way ANOVA followed by Tukey's multiple comparison test (α=0.05) using JASP software (Version 0.18.3, https://jasp-stats.org/). Statistical differences between Sdr of different materials were analyzed with 1-way ANOVA, followed by Tukey's multiple comparison test (α=0.05). Differences were considered to be statistically significant when p value was < 0.05. The effect of thermocycling on each material was evaluated using an independent student t-test between 24 h stored and thermocycled group (α=0.05). Finally, the reliability of CAD/CAM composites was studied by performing the Weibull analysis. The confidence interval was calculated based on Bütikofer et al.'s recommendations [63].

Results

One EMX sample experienced debonding before IFT testing and was excluded from the analysis (considered an outlier according to the modified Z-test score). Analysis of the specimens after the IFT test by digital microscopy did not reveal any cohesive failure of the CAD-CAM materials or Ti (Table 2). Consequently, all IFT data were included in the analysis. Typical images of the different failure modes observed are shown in Figure 4.

IFT results and Weibull modulus for each material before and after undergoing thermocycling are shown in Table 3 and Figure 5. IFT of materials ranged from 0.80 ± 0.25 to 1.10 ± 0.21 $MPa.m^{1/2}$ before thermocycling and from 0.71 ± 0.24 to 1.02 ± 0.25 $MPa.m^{1/2}$ after thermocycling. Statistical differences were only found between IFT of CER and the two top performers in each scenario (KAT and EMX before aging; KAT and ENA after aging). Indeed, prior to aging, CER was statistically inferior to EMX and KAT (-17%, $p<0.01$). After aging, CER demonstrated significantly lower IFT compared to KAT (-36%, $p=0.002$) and ENA (-18%, $p=0.013$). Thermocycling only significantly decreased IFT of EMX (-16%, $p=0.033$). Before thermocycling, there was no statistical difference in the Weibull modulus of IFT of the different groups and, therefore, the influence of thermocycling on the Weibull modulus was insignificant.

Table 4 presents the results and statistical analysis of Sdr. ENA had the highest Sdr, significantly ($p<0.05$), followed by the Ti-base and CER respectively. KAT and EMX had the lowest Sdr compared to other materials. Figure 6 presents representative images from the confocal microscope.

Discussion

The results of this study show that there is a difference in IFT of the different classes of ceramic and composite CAD-CAM materials bonded to Ti, and that aging influences EMX's IFT (Table 3 and Figure 5). Therefore, both null hypotheses are rejected.

The abovementioned differences, despite using the same cement, can be attributed to the fact that CAD-CAM material surface properties dictate the extent of mechanical and chemical bonding to cement. Regarding micromechanical retention, in EMX and ENA, it relies on roughening the surface through selective etching of the glass phase with HF. For KAT and

CER that are less etchable, sandblasting is commonly used to enhance mechanical interlocking [64–67]. According to Table 4, ENA exhibits the highest Sdr, which can be associated with the honeycomb microstructure formed after HF etching, resulting in a high level of mechanical interlocking [68]. In contrast, mechanical interlocking appears to be a less significant contributor to the adhesion of the cement to EMX and KAT, as indicated by the substantially lower Sdr values compared to the other materials. Ti and CER take a middle ground in terms of the level of the mechanical interlocking.

In terms of chemical bonding, two reactive molecules, MDP and silane, facilitate adhesion between the cement and the substrates. MDP forms P-O-Ti or P-O-Zr bonds with Ti and ZrO_2, and co-polymerizes with the composite cement through its vinyl terminal group [26,69,70]. Meanwhile, silane silanol bonds with the glass phase in EMX and ENA, co-polymerizing with the adhesive's organic phase via methacrylate functional groups [71,72]. Unlike ENA, which has an accessible glass skeleton to react with silane, the fillers of DF composites are covered by highly polymerized polymers, thus, reducing the possibility of reaction with silane molecules [72]. As a result, chemical bonding is unlikely to play a significant role in cement adhesion to CER. This point was already highlighted in previous studies, which showed that PICN materials exhibit a significantly higher IFT with etch and rinse resin cement (Variolink Esthetic Cement, Ivoclar-Vivadent, Schaan, Liechtenstein) than DF, a correlation being established with Sdr, and that silane application significantly influences IFT of PICN but not DF [67,68]. Another hypothesis is that CER, with its higher polymer content, exhibits a greater coefficient of thermal expansion, which can lead to increased stress during thermocycling, causing more pronounced degradation of IFT.

Although both KAT and EMX rely on chemical bonding, thermocycling only reduces EMX's IFT (Table 3). This could potentially be due to the hydrolysis of the silane coupling agent. This hypothesis aligns with past research indicating the limited durability of the bond between PSU

and LiSi under thermocycling, tested for up to 5000 cycles [73,74]. The P-O-Zr bond is also at risk of hydrolytic degradation [75]. However, in contrast to EMX, within the timeframe of this study, it has been concluded that achieving a stable ZrO_2-Ti adhesion using self-adhesive resin cement with MDP (PSU) is possible (Table 3). Results of previous studies analyzing the stability of this interface (when using PSU) are contradictory and are related to various aging protocols, which differ from the present study [76,77]. However, their aging protocols significantly differ from the present study.

Abovementioned discussions indicate the surface properties of CAD-CAM materials can greatly impact the behavior of their interface with titanium alloys. However, there are several other factors that affect the durability of the interface such as cement viscosity [78], chemistry of cement constituents (i.e., interaction of polar monomers with silane) [79], relative concentration of silane and MDP [80], and glass chemical composition. In fact, IFT values obtained in the present study with ENA and EMX are lower than those obtained in previous studies using the same pretreatment protocol and the same aging process but using an etch and rinse resin cement with separate silane application and bonding to the same material [68]. Therefore, other types of cements should be studied, particularly for EMX. The presence of the titanium alloy as a counterpart also clearly influences the results, as the IFT of KAT bonded to KAT counterpart with Panavia SA Cement plus (previous generation of PSU) was shown to be higher than that of KAT bonded to titanium (1.65 vs. 1.02 $MPa.m^{1/2}$) (same surface sandblasting and sample aging procedures) [32].

In this study, IFT was measured using NTP test. This method was successfully used to evaluate adhesive interfaces, and the alignment system for half-prism bonding is computer-controlled to adjust the cement thickness at 50 μm to be close to clinical situations [81,82]. The samples were tested in a water bath set at 36°C to provide a close approximation of the in-mouth conditions and to eliminate any bias resulting from temperature differences [52]. Regarding

failure mode analysis (Table 2), cohesive failure within the CAD-CAM material or Ti, or debonding from Ti can be easily detected. However, the limited contrast between the CAD-CAM material and the cement made it difficult to differentiate between debonding at the CAD-CAM material interface or within the resin cement, particularly where the remnant cement on the Ti surface was thick. Therefore, further interpretation of these data was not possible. However, the objective of the failure mode analysis with the digital microscope was only to exclude cohesive fractures from the IFT data analysis.

Future perspectives include fatigue testing of the interface to evaluate long-term performance and behavior, addressing phenomena such as subcritical crack growth.

Conclusion

CAD-CAM materials do not exhibit the same bonding properties to Ti-base materials, which could be explained by their specific surface roughness after pretreatment and their chemical affinity with the resin cement. CER had the lowest IFT both before and after thermocycling. IFT of EMX was affected by aging and the weak link could be the chemical bond, indicating that the self-adhesive resin cement used in the present study may not be indicated for this type of material, whereas KAT and ENA can rely on a more effective chemical and micromechanical bond, respectively. In any case, despite the significant roughness created on the titanium by the pre-treatment, the IFT with KAT is lower than the previously measured IFT of KAT bonded to KAT with self-adhesive resin cement, highlighting the lower bonding properties of titanium.

During the preparation of this work the authors used DeepL in order to edit the language. After using this tool, the authors reviewed and edited the content as needed and take full responsibility for the content of the publication.

References

[1] Kapos T, Evans C. CAD/CAM Technology for Implant Abutments, Crowns, and Superstructures. Int J Oral Maxillofac Implants 2014;29:117–36. https://doi.org/10.11607/jomi.2014suppl.g2.3.

[2] Makhija SK, Lawson NC, Gilbert GH, Litaker MS, McClelland JA, Louis DR, et al. Dentist material selection for single-unit crowns: Findings from the National Dental Practice-Based Research Network. J Dent 2016;55:40–7. https://doi.org/10.1016/j.jdent.2016.09.010.

[3] Lambert H, Durand J-C, Jacquot B, Fages M. Dental biomaterials for chairside CAD/CAM: State of the art. J Adv Prosthodont 2017;9:486. https://doi.org/10.4047/jap.2017.9.6.486.

[4] Ahmed KE. We're Going Digital: The Current State of CAD/CAM Dentistry in Prosthodontics. Prim Dent J 2018;7:30–5. https://doi.org/10.1177/205016841800700205.

[5] Belli R, Petschelt A, Hofner B, Hajtó J, Scherrer SS, Lohbauer U. Fracture Rates and Lifetime Estimations of CAD/CAM All-ceramic Restorations. J Dent Res 2016;95:67–73. https://doi.org/10.1177/0022034515608187.

[6] Rosentritt M, Hahnel S, Engelhardt F, Behr M, Preis V. In vitro performance and fracture resistance of CAD/CAM-fabricated implant supported molar crowns. Clin Oral Investig 2017;21:1213–9. https://doi.org/10.1007/s00784-016-1898-9.

[7] Carames J, Tovar Suinaga L, Yu YCP, Pérez A, Kang M. Clinical Advantages and Limitations of Monolithic Zirconia Restorations Full Arch Implant Supported Reconstruction: Case Series. Int J Dent 2015;2015:1–7. https://doi.org/10.1155/2015/392496.

[8] Sadid-Zadeh R, Liu P-R, Aponte-Wesson R, O'Neal SJ. Maxillary cement retained implant supported monolithic zirconia prosthesis in a full mouth rehabilitation: a clinical report. J Adv Prosthodont 2013;5:209. https://doi.org/10.4047/jap.2013.5.2.209.

[9] Coldea A, Fischer J, Swain MV, Thiel N. Damage tolerance of indirect restorative materials (including PICN) after simulated bur adjustments. Dent Mater 2015;31:684–94. https://doi.org/10.1016/j.dental.2015.03.007.

[10] Lebon N, Tapie L, Vennat E, Mawussi B. Influence of CAD/CAM tool and material on tool wear and roughness of dental prostheses after milling. J Prosthet Dent 2015;114:236–47. https://doi.org/10.1016/j.prosdent.2014.12.021.

[11] Mainjot AK, Dupont NM, Oudkerk JC, Dewael TY, Sadoun MJ. From Artisanal to CAD-CAM Blocks: State of the Art of Indirect Composites. J Dent Res 2016;95:487–95. https://doi.org/10.1177/0022034516634286.

[12] Mainjot AKJ. The One step-No prep technique: A straightforward and minimally invasive approach for full-mouth rehabilitation of worn dentition using polymer-infiltrated ceramic network (PICN) CAD-CAM prostheses. J Esthet Restor Dent 2020;32:141–9. https://doi.org/10.1111/jerd.12432.

[13] Zaghloul H, Elkassas DW, Haridy MF. Effect of incorporation of silane in the bonding agent on the repair potential of machinable esthetic blocks. Eur J Dent 2014;08:044–52. https://doi.org/10.4103/1305-7456.126240.

[14] Mainjot A. Recent advances in composite CAD/CAM blocks. Int J Esthet Dent 2016;11:275–80.

[15] Nguyen JF, Ruse D, Phan AC, Sadoun MJ. High-temperature-pressure Polymerized Resin-infiltrated Ceramic Networks. J Dent Res 2014;93:62–7. https://doi.org/10.1177/0022034513511972.

[16] Sailer I, Karasan D, Todorovic A, Ligoutsikou M, Pjetursson BE. Prosthetic failures in dental implant therapy. Periodontol 2000 2022;88:130–44. https://doi.org/10.1111/prd.12416.

[17] Chantler JGM, Evans CDJ, Zitzmann NU, Derksen W. Clinical performance of single implant prostheses restored using titanium base abutments: A systematic review and meta-analysis. Clin Oral Implants Res 2023;34:64–85. https://doi.org/10.1111/clr.14128.

[18] Lemos CAA, Verri FR, De Luna Gomes JM, Santiago Junior JF, Miyashita E, Mendonça G, et al. Survival and prosthetic complications of monolithic ceramic implant-supported single crowns and fixed partial dentures: A systematic review with meta-analysis. J Prosthet Dent 2022:S0022391322007363. https://doi.org/10.1016/j.prosdent.2022.11.013.

[19] Derksen W, Tahmaseb A, Wismeijer D. Randomized Clinical Trial comparing clinical adjustment times of CAD/CAM screw-retained posterior crowns on ti-base abutments created with digital or conventional impressions. One-year follow-up. Clin Oral Implants Res 2021;32:962–70. https://doi.org/10.1111/clr.13790.

[20] Koenig V, Wulfman C, Bekaert S, Dupont N, Le Goff S, Eldafrawy M, et al. Clinical behavior of second-generation zirconia monolithic posterior restorations: Two-year results of a prospective study with Ex vivo analyses including patients with clinical signs of bruxism. J Dent 2019;91:103229. https://doi.org/10.1016/j.jdent.2019.103229.

[21] Lambert F, Eldafrawy M, Bekaert S, Mainjot A. One-tooth one-time (1T1T), immediate loading of posterior single implants with the final crown: 2-year results of a case series. Int J Oral Implantol 2020;13:369–83.

[22] Pitta J, Burkhardt F, Mekki M, Fehmer V, Mojon P, Sailer I. Effect of airborne-particle abrasion of a titanium base abutment on the stability of the bonded interface and retention forces of crowns after artificial aging. J Prosthet Dent 2021;126:214–21. https://doi.org/10.1016/j.prosdent.2020.06.013.

[23] Krejci I, Daher R. Stress distribution difference between Lava Ultimate full crowns and IPS e.max CAD full crowns on a natural tooth and on tooth-shaped implant abutments. Odontology 2017;105:254–6. https://doi.org/10.1007/s10266-016-0276-z.

[24] Matinlinna JP. Processing and bonding of dental ceramics. Non-Met. Biomater. Tooth Repair Replace., Elsevier; 2013, p. 129–60. https://doi.org/10.1533/9780857096432.2.129.

[25] Matinlinna JP, Lung CYK, Tsoi JKH. Silane adhesion mechanism in dental applications and surface treatments: A review. Dent Mater 2018;34:13–28. https://doi.org/10.1016/j.dental.2017.09.002.

[26] Serichetaphongse P, Chitsutheesiri S, Chengprapakorn W. Comparison of the shear bond strength of composite resins with zirconia and titanium using different resin cements. J Prosthodont Res 2022;66:109–16. https://doi.org/10.2186/jpr.JPR_D_20_00299.

[27] Maravić T, Mazzitelli C, Mancuso E, Del Bianco F, Josić U, Cadenaro M, et al. Resin composite cements: Current status and a novel classification proposal. J Esthet Restor Dent 2023;35:1085–97. https://doi.org/10.1111/jerd.13036.

[28] Yoshihara K, Nagaoka N, Sonoda A, Maruo Y, Makita Y, Okihara T, et al. Effectiveness and stability of silane coupling agent incorporated in ‘universal’ adhesives. Dent Mater 2016;32:1218–25. https://doi.org/10.1016/j.dental.2016.07.002.

[29] Yao C, Yu J, Wang Y, Tang C, Huang C. Acidic pH weakens the bonding effectiveness of silane contained in universal adhesives. Dent Mater 2018;34:809–18. https://doi.org/10.1016/j.dental.2018.02.004.

[30] Yoshihara K, Nagaoka N, Maruo Y, Nishigawa G, Yoshida Y, Van Meerbeek B. Silane-coupling effect of a silane-containing self-adhesive composite cement. Dent Mater 2020;36:914–26. https://doi.org/10.1016/j.dental.2020.04.014.

[31] Dimitriadi M, Petropoulou A, Vakou D, Zinelis S, Eliades G. In vitro evaluation of a silane containing self-adhesive resin luting agent. Dent Mater 2023;39:181–91. https://doi.org/10.1016/j.dental.2022.12.007.

[32] Eldafrawy M, Bekaert S, Nguyen J-F, Sadoun M, Mainjot A. Bonding properties of third-generation zirconia CAD-CAM blocks for monolithic restorations to composite and resin-modified glass-ionomer cements. J Prosthodont Res 2022;66:466–75. https://doi.org/10.2186/jpr.JPR_D_21_00044.

[33] Zahoui A, Bergamo E, Marun M, Silva K, Coelho P, Bonfante E. Cementation Protocol for Bonding Zirconia Crowns to Titanium Base CAD/CAM Abutments. Int J Prosthodont 2020;33:527–35. https://doi.org/10.11607/ijp.6696.

[34] Hansen NA, Wille S, Kern M. Effect of reduced airborne-particle abrasion pressure on the retention of zirconia copings resin bonded to titanium abutments. J Prosthet Dent 2020;124:60–7. https://doi.org/10.1016/j.prosdent.2019.07.001.

[35] Lang R, Hiller K-A, Kienböck L, Friedl K, Friedl K-H. Influence of autoclave sterilization on bond strength between zirconia frameworks and Ti-base abutments using different resin cements. J Prosthet Dent 2022;127:617.e1-617.e6. https://doi.org/10.1016/j.prosdent.2022.01.028.

[36] Wiedenmann F, Liebermann A, Spintzyk S, Eichberger M, Stawarczyk B. Influence of Different Cleaning Procedures on Tensile Bond Strength Between Zirconia Abutment and Titanium Base. Int J Oral Maxillofac Implants 2019;34:1318–27. https://doi.org/10.11607/jomi.7638.

[37] T. P. Bergamo E, Zahoui A, Luri Amorin Ikejiri L, Marun M, Peixoto Da Silva K, G. Coelho P, et al. Retention of zirconia crowns to Ti-base abutments: effect of luting protocol, abutment treatment and autoclave sterilization. J Prosthodont Res 2021;65:171–5. https://doi.org/10.2186/jpr.JPOR_2019_537.

[38] Mehl C, Zhang Q, Lehmann F, Kern M. Retention of zirconia on titanium in two-piece abutments with self-adhesive resin cements. J Prosthet Dent 2018;120:214–9. https://doi.org/10.1016/j.prosdent.2017.11.020.

[39] Arce C, Lawson N, Liu P-R, Lin C, Givan D. Retentive Force of Zirconia Implant Crowns on Titanium Bases Following Different Surface Treatments. Int J Oral Maxillofac Implants 2018;33:530–5. https://doi.org/10.11607/jomi.5915.

[40] Burkhardt F, Pitta J, Fehmer V, Mojon P, Sailer I. Retention Forces of Monolithic CAD/CAM Crowns Adhesively Cemented to Titanium Base Abutments—Effect of Saliva Contamination Followed by Cleaning of the Titanium Bond Surface. Materials 2021;14:3375. https://doi.org/10.3390/ma14123375.

[41] Nouh I, Kern M, Sabet AE, Aboelfadl AK, Hamdy AM, Chaar MS. Mechanical behavior of posterior all-ceramic hybrid-abutment-crowns versus hybrid-abutments with separate crowns—A laboratory study. Clin Oral Implants Res 2019;30:90–8. https://doi.org/10.1111/clr.13395.

[42] Burkhardt F, Sailer I, Fehmer V, Mojon P, Pitta J. Retention and Marginal Integrity of CAD/CAM Fabricated Crowns Adhesively Cemented to Titanium Base Abutments—Influence of Bonding System and Restorative Material. Int J Prosthodont 2023;36. https://doi.org/10.11607/ijp.7576.

[43] Rödiger M, Kloß J, Gersdorff N, Bürgers R, Rinke S. Removal forces of adhesively and self-adhesively luted implant-supported zirconia copings depend on abutment geometry.

J Mech Behav Biomed Mater 2018;87:119–23. https://doi.org/10.1016/j.jmbbm.2018.07.028.

[44] Rödiger M, Rinke S, Ehret-Kleinau F, Pohlmeyer F, Lange K, Bürgers R, et al. Evaluation of removal forces of implant-supported zirconia copings depending on abutment geometry, luting agent and cleaning method during re-cementation. J Adv Prosthodont 2014;6:233. https://doi.org/10.4047/jap.2014.6.3.233.

[45] De Jager N, Pallav P, Feilzer AJ. The influence of design parameters on the FEA-determined stress distribution in CAD–CAM produced all-ceramic dental crowns. Dent Mater 2005;21:242–51. https://doi.org/10.1016/j.dental.2004.03.013.

[46] Karaokutan I, Ozel GS. Effect of surface treatment and luting agent type on shear bond strength of titanium to ceramic materials. J Adv Prosthodont 2022;14:78. https://doi.org/10.4047/jap.2022.14.2.78.

[47] Guilherme N, Wadhwani C, Zheng C, Chung K-H. Effect of surface treatments on titanium alloy bonding to lithium disilicate glass-ceramics. J Prosthet Dent 2016;116:797–802. https://doi.org/10.1016/j.prosdent.2016.04.023.

[48] Amornwichitwech L, Palanuwech M. Shear Bond Strength of Lithium Disilicate Bonded with Various Surface-Treated Titanium. Int J Dent 2022;2022:1–11. https://doi.org/10.1155/2022/4406703.

[49] Scherrer SS, Cesar PF, Swain MV. Direct comparison of the bond strength results of the different test methods: A critical literature review. Dent Mater 2010;26:e78–93. https://doi.org/10.1016/j.dental.2009.12.002.

[50] Van Meerbeek B, Peumans M, Poitevin A, Mine A, Van Ende A, Neves A, et al. Relationship between bond-strength tests and clinical outcomes. Dent Mater 2010;26:e100–21. https://doi.org/10.1016/j.dental.2009.11.148.

[51] Armstrong S, Geraldeli S, Maia R, Raposo LHA, Soares CJ, Yamagawa J. Adhesion to tooth structure: A critical review of “micro” bond strength test methods. Dent Mater 2010;26:e50–62. https://doi.org/10.1016/j.dental.2009.11.155.

[52] Soderholm K-J. Review of the fracture toughness approach. Dent Mater 2010;26:e63–77. https://doi.org/10.1016/j.dental.2009.11.151.

[53] De Munck J, Luehrs A-K, Poitevin A, Van Ende A, Van Meerbeek B. Fracture toughness versus micro-tensile bond strength testing of adhesive–dentin interfaces. Dent Mater 2013;29:635–44. https://doi.org/10.1016/j.dental.2013.03.010.

[54] Pongprueksa P, De Munck J, Karunratanakul K, Barreto BC, Van Ende A, Senawongse P, et al. Dentin Bonding Testing Using a Mini-interfacial Fracture Toughness Approach. J Dent Res 2016;95:327–33. https://doi.org/10.1177/0022034515618960.

[55] Cesar PF, Della Bona A, Scherrer SS, Tholey M, Van Noort R, Vichi A, et al. ADM guidance—Ceramics: Fracture toughness testing and method selection. Dent Mater 2017;33:575–84. https://doi.org/10.1016/j.dental.2017.03.006.

[56] Ruse ND, Troczynski T, MacEntee MI, Feduik D. Novel fracture toughness test using a notchless triangular prism (NTP) specimen. J Biomed Mater Res 1996;31:457–63. https://doi.org/10.1002/(SICI)1097-4636(199608)31:4<457::AID-JBM4>3.0.CO;2-K.

[57] Mesmar S, Ruse ND. Interfacial Fracture Toughness of Adhesive Resin Cement—Lithium-Disilicate/Resin-Composite Blocks. J Prosthodont 2019;28. https://doi.org/10.1111/jopr.12672.

[58] Ilie N, Ruse ND. Shear bond strength vs interfacial fracture toughness — Adherence to CAD/CAM blocks. Dent Mater 2019;35:1769–75. https://doi.org/10.1016/j.dental.2019.10.003.

[59] De Munck J, Van Landuyt K, Peumans M, Poitevin A, Lambrechts P, Braem M, et al. A Critical Review of the Durability of Adhesion to Tooth Tissue: Methods and Results. J Dent Res 2005;84:118–32. https://doi.org/10.1177/154405910508400204.

[60] Armstrong S, Breschi L, Özcan M, Pfefferkorn F, Ferrari M, Van Meerbeek B. Academy of Dental Materials guidance on in vitro testing of dental composite bonding effectiveness to dentin/enamel using micro-tensile bond strength (μTBS) approach. Dent Mater 2017;33:133–43. https://doi.org/10.1016/j.dental.2016.11.015.

[61] Munz D, Fett T. Ceramics: mechanical properties, failure behaviour, materials selection. Berlin Heidelberg: Springer-Verlag; 2001.

[62] Zorzin J, Beck S, Belli R, Petschelt A, Boccaccini AR, Lohbauer U. Adhesion and interfacial characterization of biomimetically texturized lithium disilicate. Int J Adhes Adhes 2019;91:131–41. https://doi.org/10.1016/j.ijadhadh.2019.03.012.

[63] Bütikofer L, Stawarczyk B, Roos M. Two regression methods for estimation of a two-parameter Weibull distribution for reliability of dental materials. Dent Mater 2015;31:e33–50. https://doi.org/10.1016/j.dental.2014.11.014.

[64] Fathi A, Hashemi S, Tabatabaei S, Mosharraf R, Atash R. Adhesion to Zirconia: An umbrella review. Int J Adhes Adhes 2023;122:103322. https://doi.org/10.1016/j.ijadhadh.2023.103322.

[65] Mine A, Kabetani T, Kawaguchi-Uemura A, Higashi M, Tajiri Y, Hagino R, et al. Effectiveness of current adhesive systems when bonding to CAD/CAM indirect resin materials: A review of 32 publications. Jpn Dent Sci Rev 2019;55:41–50. https://doi.org/10.1016/j.jdsr.2018.10.001.

[66] Yoshihara K, Nagaoka N, Maruo Y, Nishigawa G, Irie M, Yoshida Y, et al. Sandblasting may damage the surface of composite CAD–CAM blocks. Dent Mater 2017;33:e124–35. https://doi.org/10.1016/j.dental.2016.12.003.

[67] Eldafrawy M, Greimers L, Bekaert S, Gailly P, Lenaerts C, Nguyen J-F, et al. Silane influence on bonding to CAD-CAM composites: An interfacial fracture toughness study. Dent Mater 2019;35:1279–90. https://doi.org/10.1016/j.dental.2019.05.019.

[68] Eldafrawy M, Ebroin MG, Gailly PA, Nguyen J-F, Sadoun MJ, Mainjot AK. Bonding to CAD-CAM Composites: An Interfacial Fracture Toughness Approach. J Dent Res 2018;97:60–7. https://doi.org/10.1177/0022034517728714.

[69] Özcan M, Nijhuis H, Valandro LF. Effect of Various Surface Conditioning Methods on the Adhesion of Dual-cure Resin Cement with MDP Functional Monomer to Zirconia after Thermal Aging. Dent Mater J 2008;27:99–104. https://doi.org/10.4012/dmj.27.99.

[70] Tsuchimoto Y, Yoshida Y, Mine A, Nakamura M, Nishiyama N, Van Meerbeek B, et al. Effect of 4-MET- and 10-MDP-based Primers on Resin Bonding to Titanium. Dent Mater J 2006;25:120–4. https://doi.org/10.4012/dmj.25.120.

[71] Tian T, Tsoi JK-H, Matinlinna JP, Burrow MF. Aspects of bonding between resin luting cements and glass ceramic materials. Dent Mater 2014;30:e147–62. https://doi.org/10.1016/j.dental.2014.01.017.

[72] Yano HT, Ikeda H, Nagamatsu Y, Masaki C, Hosokawa R, Shimizu H. Correlation between microstructure of CAD/CAM composites and the silanization effect on adhesive bonding. J Mech Behav Biomed Mater 2020;101:103441. https://doi.org/10.1016/j.jmbbm.2019.103441.

[73] Willers AE, Gomes Araújo-Neto V, Bosso André C, Giannini M. Bond durability of a silane-containing self-adhesive and conventional resin cements to CAD/CAM glass and hybrid ceramics. J Adhes Sci Technol 2023:1–14. https://doi.org/10.1080/01694243.2023.2229696.

[74] Murakami S, Hirano K, Fusejima F. Bonding Durability of Resin Cement to Lithium Disilicate Glass Ceramics. Dent Mater 2022;38:e31. https://doi.org/10.1016/j.dental.2021.12.081.

[75] Chen C, Chen Y, Lu Z, Qian M, Xie H, Tay FR. The effects of water on degradation of the zirconia-resin bond. J Dent 2017;64:23–9. https://doi.org/10.1016/j.jdent.2017.04.004.

[76] Soto-Montero J, Missiato AV, Dias CTDS, Giannini M. Effect of airborne particle abrasion and primer application on the surface wettability and bond strength of resin cements to translucent zirconia. J Adhes Sci Technol 2023;37:1458–70. https://doi.org/10.1080/01694243.2022.2079326.

[77] Bagegni A, Borchers J, Beisel S, Patzelt SBM, Vach K, Kohal R. Bonding Strength of Various Luting Agents between Zirconium Dioxide Crowns and Titanium Bonding Bases after Long-Term Artificial Chewing. Materials 2023;16:7314. https://doi.org/10.3390/ma16237314.

[78] Dapieve KS, Pilecco RO, Temp RW, Villetti MA, Pereira GKR, Valandro LF. Adhesion to lithium disilicate glass-ceramics after aging: Resin viscosity and ceramic surface treatment effects. J Mech Behav Biomed Mater 2023;142:105819. https://doi.org/10.1016/j.jmbbm.2023.105819.

[79] Farahani M, Wallace WE, Antonucci JM, Guttman CM. Analysis by mass spectrometry of the hydrolysis/condensation reaction of a trialkoxysilane in various dental monomer solutions. J Appl Polym Sci 2006;99:1842–7. https://doi.org/10.1002/app.22190.

[80] Koko M, Takagaki T, Abdou A, Inokoshi M, Ikeda M, Wada T, et al. Effects of the ratio of silane to 10-methacryloyloxydecyl dihydrogenphosphate (MDP) in primer on bonding performance of silica-based and zirconia ceramics. J Mech Behav Biomed Mater 2020;112:104026. https://doi.org/10.1016/j.jmbbm.2020.104026.

[81] Hung SH, Hung K-S, Eick JD, Chappell RP. Marginal fit of porcelain-fused-to-metal and two types of ceramic crown. J Prosthet Dent 1990;63:26–31. https://doi.org/10.1016/0022-3913(90)90260-J.

[82] Moraes R, Boscato N, Jardim P, Schneider L. Dual and Self-curing Potential of Self-adhesive Resin Cements as Thin Films. Oper Dent 2011;36:635–42. https://doi.org/10.2341/10-367-L.

Legends of Figures

Figure 1. Study summary (A) Sample preparation; (B) Study design: sample groups; (C) Study design: experimentations.

Figure 2. Schema that shows the NTP apparatus in motion with a prism fixed inside. The arrows pointing in opposite directions show that a tensile force is being applied to the bonded interface, which causes cracks to start at the tip of the prism and propagate until bond failures.

Figure 3. (A-B) Cohesive failure within one material, either the substrate or resin cement; (C-D) Adhesive failure refers to the complete detachment of a resin cement from the interface of Ti-base and CAD-CAM materials respectively; (E) Adhesive failure refers to the partial separation of the resin cement from one (or both) substrate interfaces (the crack propagates along either the red or green dashed line). (F) Mixed mode, in which crack propagation happens through both the CAD-CAM material and resin cement, resulting in a fractured surface that has residual CAD-CAM material (modified from [62]).

Figure 4. Digital microscopy (x30 magnification) of the Ti prism after the IFT test to identify the failure mode (A, B, C: crack initiation on the right). (A) Crack propagation through the resin cement (cohesive failure in the resin cement) (EMX). (B) At the resin-cement-Ti interface (adhesive failure) (ENA). (C) Partial separation at the resin-cement-Ti interface (adhesive failure) (CER). (D) Mixed mode failure with CAD-CAM composite remaining at the Ti interface (ENA).

Figure 5. Raincloud plots of IFT for the 4 different groups of materials. The subscript 24 implies after 24 h of storage; the subscript 10000 means after 10000 cycles thermocycling. Significant statistical differences are present on the left (1-way ANOVA except between aging and without aging which is an independent t-test), n=20 per group.

Figure 6. Confocal laser microscopy images of materials following specific pretreatment, with areas exhibiting negative values depicted in blue and positive values in red. Images show (A) CER; (B) EMX; (C) ENA; (D) KAT; and (E) Ti.

Legends of Tables

Table 1. Materials used in the study and their compositions.

Table 2. Failure pattern of the interfaces (frequency)

Table 3. Descriptive and Weibull analysis of IFT for the 4 different groups of materials.

Table 4. Representative means ± standard deviations of Sdr of each material.

Figure 1

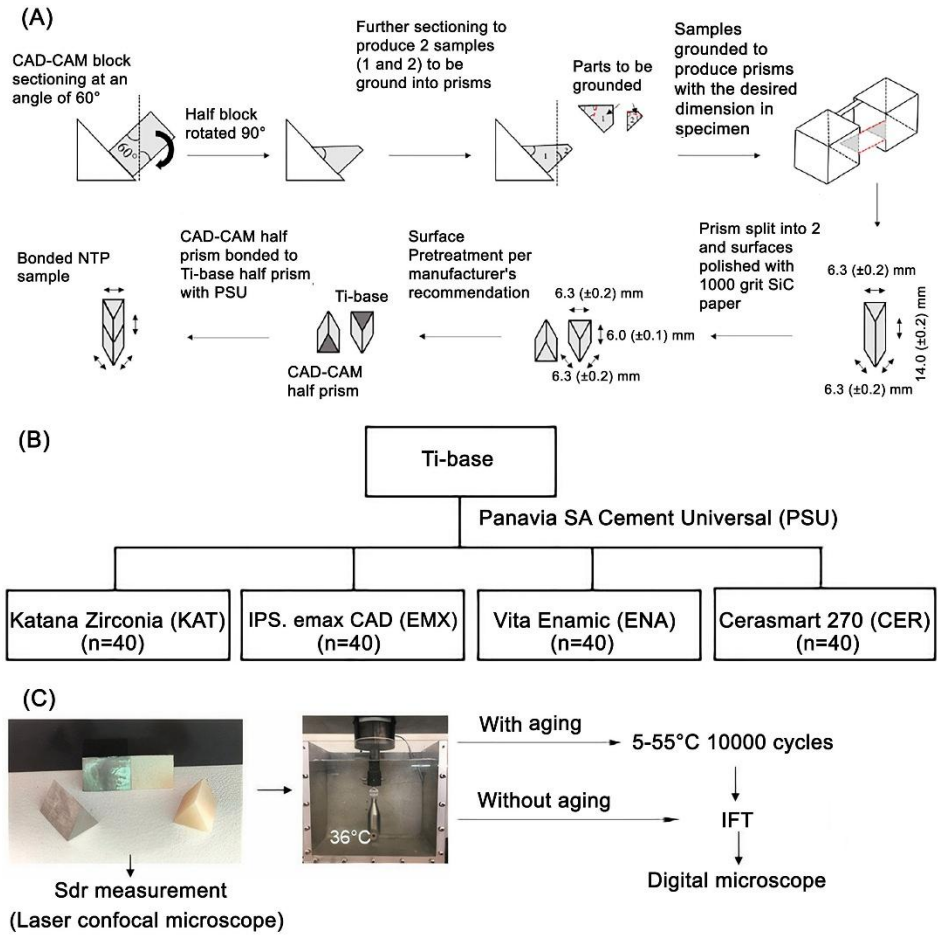
(A)
CAD-CAM block sectioning at an angle of 60°
60°
Half block rotated 90°
Further sectioning to produce 2 samples (1 and 2) to be ground into prisms
Parts to be grounded
Samples grounded to produce prisms with the desired dimension in specimen
Prism split into 2 and surfaces polished with 1000 grit SiC paper
6.3 (±0.2) mm
14.0 (±0.2) mm
6.3 (±0.2) mm
Surface Pretreatment per manufacturer's recommendation
6.3 (±0.2) mm
6.0 (±0.1) mm
6.3 (±0.2) mm
CAD-CAM half prism bonded to Ti-base half prism with PSU
Ti-base
CAD-CAM half prism
Bonded NTP sample
(B)
Ti-base
Panavia SA Cement Universal (PSU)
Katana Zirconia (KAT) (n=40)
IPS. emax CAD (EMX) (n=40)
Vita Enamic (ENA) (n=40)
Cerasmart 270 (CER) (n=40)
(C)
With aging
5-55°C 10000 cycles
Without aging
IFT
36°C
Digital microscope
Sdr measurement
(Laser confocal microscope)

Figure 2

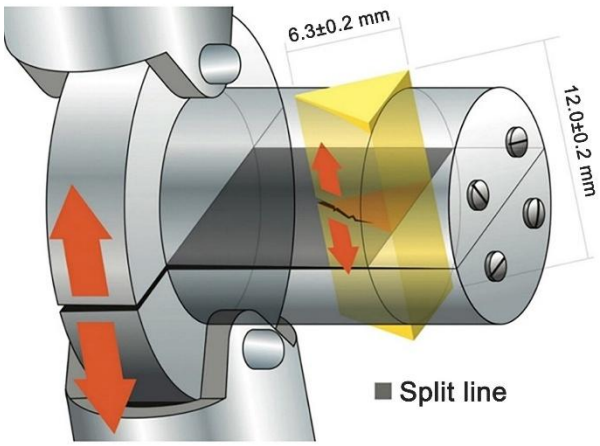

Figure 3

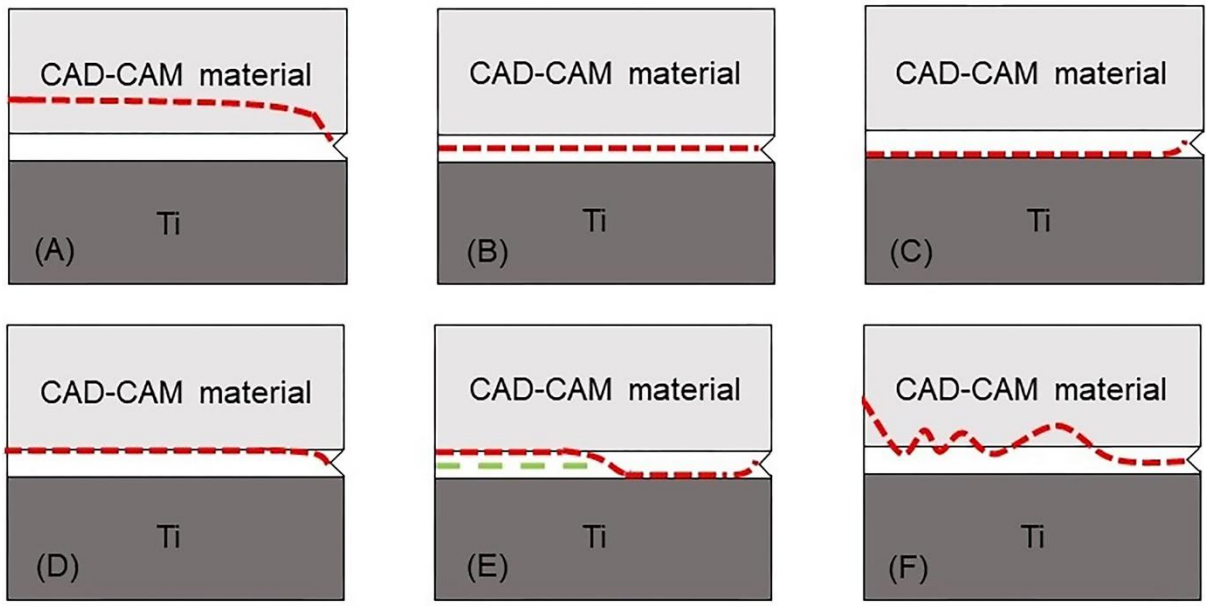
CAD-CAM material
Ti
(A)
CAD-CAM material
Ti
(B)
CAD-CAM material
Ti
(C)
CAD-CAM material
Ti
(D)
CAD-CAM material
Ti
(E)
CAD-CAM material
Ti
(F)

Figure 4

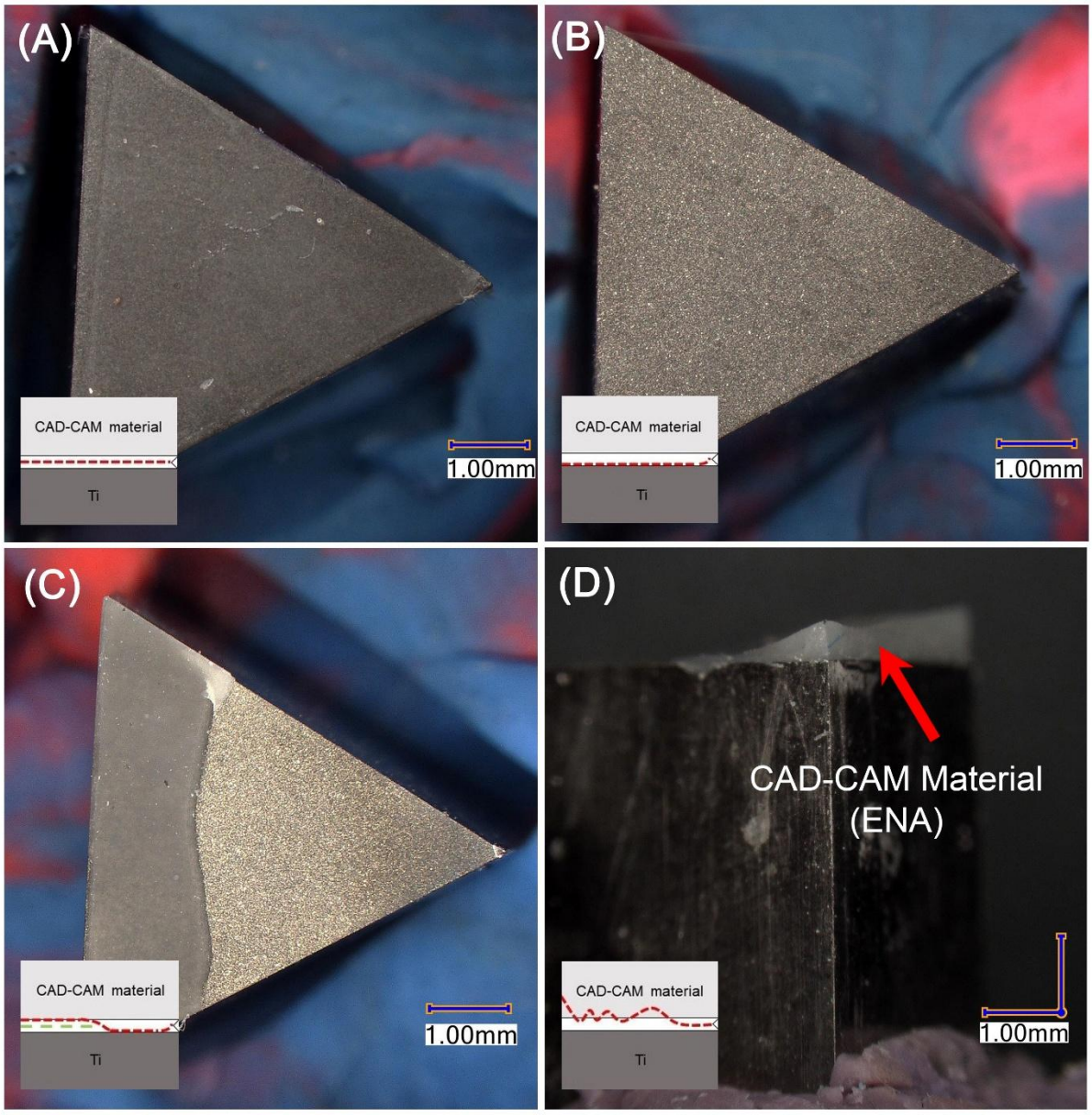
(A)
CAD-CAM material
Ti
1.00mm
(B)
CAD-CAM material
Ti
1.00mm
(C)
CAD-CAM material
Ti
1.00mm
(D)
CAD-CAM Material
(ENA)
CAD-CAM material
Ti
1.00mm

Figure 5

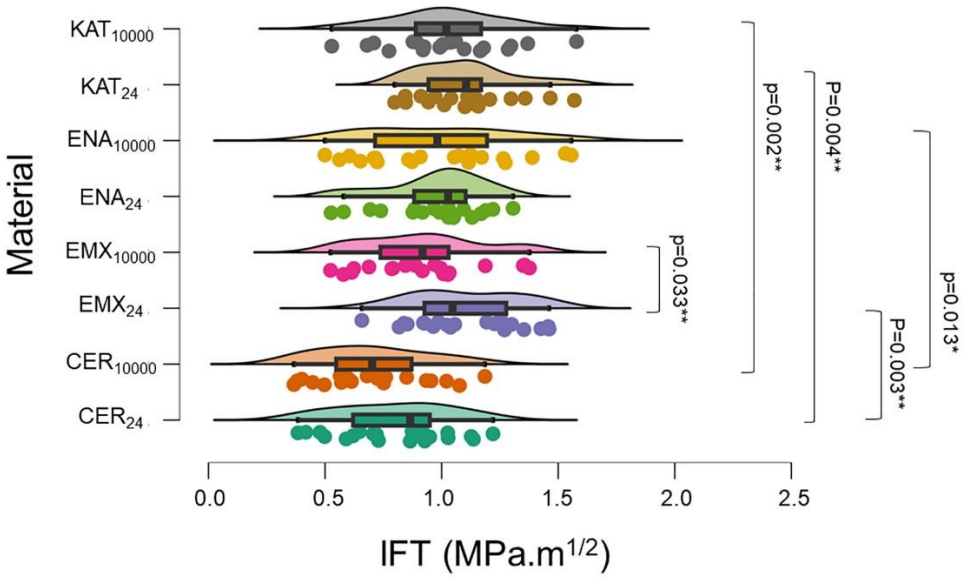

Figure 6

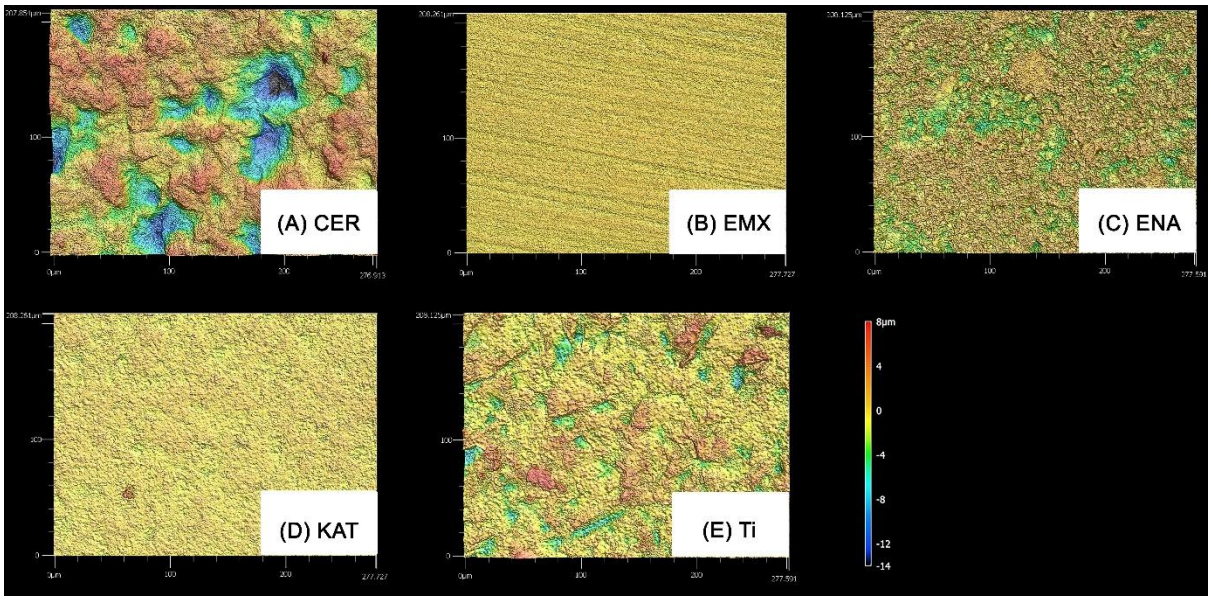

Table 1

Material	Composition (weight %)	Manufacturer
Titanium-base (Ti-base)	Ti (89.4%), Al (6.2%), V (4%), N, C, H, Fe, O (<0.4%)	Scheftner Dental Alloys (Mainz, Germany)
Katana Zirconia blocks (KAT)	ZrO_2, (10wt%; 5mol%) Y_2O_3	Kuraray Noritake (Tokyo, Japan)
IPS. emax CAD (EMX)	SiO_2 (57–80 %), Li_2O (11–19 %), other oxides	Ivoclar Vivadent (Schaan, Liechtenstein)
Vita Enamic (ENA)	Glass-ceramic sintered network (86%), UDMA, TEGDMA	Vita Zahnfabrik (Bad Sackingen, Germany)
Cerasmart 270 (CER)	Inorganic fillers: Barium glass (300 nm), silica (20 nm) (71wt%) Organic matrix: Bis-MEPP, UDMA, DMA	GC corporation (Tokyo, Japan)
Panavia SA Cement Universal (PSU)	Paste A: 10-MDP, Bis-GMA, TEGDMA, 2-HEMA, hydrophobic aromatic dimethacrylate, , silanated barium glass filler, silanated colloidal silica, dl Camphorquinone, peroxide, catalysts, pigments Paste B: hydrophobic aromatic dimethacrylate, hydrophobic aliphatic dimethacrylate, silanated barium glass filler, surface treated sodium fluoride, accelerators, pigments, silane coupling agent	Kuraray Noritake (Tokyo, Japan)

10-MDP : 10- methacryloyloxydecyl dihydrogen phosphate; BisGMA: Bisphenol glycidyl dimethacrylate; TEGDMA: Triethylene glycol dimethacrylate; 2-HEMA: 2-Hydroxyethyl methacrylate; UDMA: Urethane dimethacrylate; Bis-MEPP: 2,2-Bis(4-methacryloxypolyethoxyphenyl) propane; SiO_2 Silicon oxide; Al_2O_3: Aluminium oxide; Li_2O: Lithium oxide

Table 2

Materials	Cohesive (CAD-CAM)	Cohesive cement	Adhesive (Ti)	Adhesive (CAD-CAM)	Adhesive (mixed)	Mixed mode	Undetermined
CER_{24}	0	0	1	0	9	4	6
EMX_{24}	0	4	1	0	3	0	12
ENA_{24}	0	4	1	0	11	2	2
KAT_{24}	0	2	1	0	3	0	14
CER_{10000}	0	7	1	0	7	3	2
EMX_{10000}	0	11	1	0	5	0	3
ENA_{10000}	0	2	4	0	10	3	1
KAT_{10000}	0	5	0	0	4	0	11

Cohesive (CAD-CAM): Failure within CAD-CAM material; Cohesive cement: Failure within cement; Adhesive (Ti): Complete adhesive failure from Ti-base interface; Adhesive (CAD-CAM): Complete adhesive failure from CAD-CAM interface; Adhesive (mixed): Partial adhesive separation at substrate interfaces; Mixed mode: Crack propagation through both CAD-CAM and adhesive; Undetermined: Falls under Adhesive (Ti), Adhesive (CAD-CAM), Adhesive (mixed), or Mixed mode but cannot be conclusively identified. The subscript 24 implies after 24 hours of storage; the subscript 10000 means after 10000 cycles thermocycling.

Table 3

Materials	IFT_{24}	IFT_{10000}	P value	Weibull $modulus_{24}$ (95%CI)	Weibull $modulus_{10000}$ (95%CI)
CER	0.80 ± 0.25^{b}	0.71 ± 0.24^{b}	0.24	3.44 (2.17-5.44)	3.05 (1.93-4.83)
EMX	1.10 ± 0.24^{a}	0.92 ± 0.26^{ab}	0.03^{*}	4.84 (3.06- 7.66)	3.64 (2.28-5.84)
ENA	$0.97\pm 0.21^{a,b}$	0.98 ± 0.32^{a}	0.91	4.40 (2.78-6.97)	3.28 (2.07-5.02)
KAT	1.10 ± 0.21^{a}	1.02 ± 0.25^{a}	0.29	5.73 (3.61-9.07)	4.16 (2.63-6.58)

Different superscript letters indicate statistical differences inside the respective column. The subscript 24 implies after 24 hours of storage; the subscript 10000 means after 10000 cycles of thermocycling. For the Weibull modulus, the overlap of the confidence interval is considered to be no statistical difference.

Table 4

Material	Sdr (%)
Ti-base	496.9 ± 28.5^{b}
ENA	759.6 ± 53.8^{a}
CER	285.2 ± 21.0^{c}
EMX	95.6 ± 15.5^{d}
KAT	109.2 ± 30.9^{d}

The same superscript letters indicate statistically same material (1-way analysis of variance followed by Tukey's test, $\alpha = 0.05$).